International Research Journal of Engineering and Technology (IRJET) e-ISSN: 2395-0056
Volume: 06 Issue: 04 | Apr 2019 www.irjet.net p-ISSN: 2395-0072

ANALYSIS AND COMPARISON OF FRICTION STIR WELDING ON VARIOUS ALUMINUM ALLOYS

Krishnakumar G[1], Dhanapal A[2] RajaMohan M[3] Deepak lawrance G[4]

[1]*Dept. of mechanical Engineering, Sri Ramanujar Engineering college, kolappakam, Chennai, Tamil Nadu, India*
[2]*Principal of Sri Ramanujar Engineering college, Chennai, Tamil Nadu, India*
[3]*Head of Dept. of mechanical Engineering, Sri Ramanujar Engineering college, Chennai, Tamil Nadu, India*
[4]*Asst .professor, Dept. of mechanical Engineering, Sri Ramanujar Engineering college, Chennai, Tamil Nadu, India*

Abstract - *Friction stir welding a solid-state joining technique, is being extensively as dissimilar joining of Al, Mg, Cu, Ti, and their alloys. In FSW of two Aluminium alloys-AI 5083 and AI 7075- at various combinations of tool rotation speeds and tool traverse speeds. the macrostructure and microstructure clearly showed typical zones of a FSW joint and the appropriate grain sizes. A coupled thermo-mechanical model was developed to study the temperature fields under different rotating speeds, (300, 400 and 500) r/min, during the FSW process of the plunge stage. The weldability of Al 5083 and Al 7075 Aluminium alloys, which are widely used in welding fabrication, is compared by analyzing the welds obtained from both materials under a large range of welding conditions (varying tool dimensions, rotation and traverse speeds, axial loads and tilt angles) chosen to ensure high welding speeds.*

Keywords: *friction-stir welding, high strength and speed, welding parameters, metallography, mechanical test.*

1. INTRODUCTION

FSP expands the innovation of friction stir welding (FSW) developed by The Welding Institute (TWI) of United Kingdom in 1991 to develop local and surface properties at selected locations. In the present work, FSP is investigated as a potential processing technique for aluminum alloys. Preliminary studies of different FS processed alloys report the processed zone to contain fine grained, homogeneous and equiaxed microstructure. Several studies have been conducted to optimize the process and relate various process parameters like rotational and translational speeds to resulting microstructure. But there is only a little data reported on the effect of the process parameters on the forces generated during processing, and the resulting microstructure of aluminum alloys especially AI 5083 and AI 7075 which is a potential superplastic alloy.

FSW joint in aluminum alloys consists of four major microstructural. The heat-affected zone (HAZ) lies close to the weld center. The material has experienced a thermal cycle, so the modifications in mechanical properties and in the microstructure are noticed. However, no plastic deformation occurs in this zone. The thermo-mechanically affected zone has been plastically deformed by the FSW is a very modern welding process with a great future use, primarily due to a variety of possible combinations of dissimilar materials to be welded and the possibility to be controlled efficiently and the heat from the process also exerts some influence on the material. FSW can be used for joining many types of materials and material combinations: aluminum and its alloys, copper and its alloys, lead-magnesium alloys, magnesium and aluminum, zinc, titanium and its alloys, mild steel and metal matrix composites (MMCs) based on aluminum and plastics. Compared with the conventional welding techniques, FSW possesses many advantages, such as the absence of melting, a low number of defects, low distortion, etc.

In the present work, sheets of aluminum alloys AI 5083 and AI7075 were friction stir processed under various combinations of rotational and translational speeds. The processing forces were measured during the process and the resulting microstructure was analyzed. The results indicate that the processing forces and the microstructure evolved during FSP are sensitive to the rotational and translational speed. It is observed that the forces generated increase with the increasing rotational speed. The grain refinement was observed to vary directly with rotational speed and inversely with the translational speed. Also these forces generated were proportional to the grain refinement i.e., greater refinement of grains occurred at lower forces. Thus the choice of process parameters especially the rotational speed has a significant effect on the control and optimization of the process.

2. EXPERIMENTAL

In the present friction stir welding studies, two commercial aluminium alloys AI 5083 and AI 7075 were used-former being a partially recrystallized solid solution-strengthened aluminium alloy and latter being a precipitate-hardened aluminium alloy. The AI 5083 was in the solutionized condition (solution heat treated at 530°C for duration of 0.5 h, followed by water quenching), whereas the AI 7075 was in the as received state.

Table 1 Mechanical properties of Aluminum alloys

S.No	Alloy	UTS (MPa)	YS (MPa)	Elongation (%)	Hardness (VHN)
1.	AI 5083	262	214	10	80
2.	AI 7075	310	276	12	107

The FSW experiments were carried out using dedicated locally designed and fabricated friction stir welding equipment. During the experiments, a data logger was used to collect the data (consisting of normal load, traverse load, spindle torque, etc.) from load cells attached to the equipment. The dimensions of the workpieces used were 300 mm× 50 mm × 5 mm. Prior to welding, one side of the workpieces was machined in the transverse long section plane (length-thickness plane) using a milling equipment. This facilitated a good contact of the mating surfaces with each other when arranged in a butt configuration.

The workpieces were cleaned thoroughly by acetone to remove any dirt, organic material, and fine particles left after the machining process. A commercial high speed steel (HSS) tool, having a cylindrical geometry with 4.8 mm pin length and 6 mm pin diameter and having 5 mm shoulder diameter was used. The tool tilt was kept constant at 3° for all welding trials. Several FSW trials were carried out at 1120 and 1400 rpm and for various traverse speeds ranging from 60 mm/min, 80 mm/min and 100 mm/min. Depending on the combination of tool rotation speed and tool traverse speed used, the specimens were assigned identities according to the nomenclature The qualification of defect-free joints was done using X-ray radiography and dye penetration tests. It was observed that for R1400F080 specimen (welded at tool rotation speed of 1400 rpm and tool traverse speed of 80 mm/min) defect-free joints were obtained all along the interface.

2.1 Preparation of the welding plate

Fig 1 Thermally processed and machine for FSW 180 mm x65mmx5mm

Fig 2 A specimen for sample making was a panel with the dimensions of 680 mm × 580 mm × 13 mm

A specimen for sample making was a panel with the dimensions of 680 mm × 580 mm × 13 mm a hardness of 175 HB, and made Fig-2 Specimen for sample making with the dimensions of 680mm x580mm x13mm of raw aluminium, where the alloying elements were added as clean metal alloys, or master alloys. It passed all phases of the technological procedure: thermo-mechanical processing, casting of a raw billet, two-level homogenization, cutting and preparation for forging, free forging and forging in a tool, hardening, pressing of 1 % and 3 %, and artificial ageing. To eliminate the potential heat influence on the initial microstructure and on the experimental results, the panels were cut with a water jet and afterwards skimmed of saw chips, and made in specified measurements with an intensive cooling of the treated surface.

2.2 Equipment for the procedure implementation, tools and process parameters

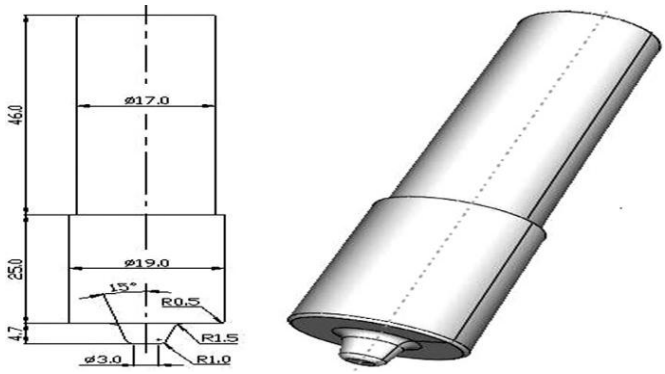

Fig 3 Welding tool use for the experiment and numerical analysis

The pieces were fastened to the backing plate without turning down the edges and after that the vertical head of the milling machine, with the inserted tool in the tapered elastic capsule, was placed in the contact position on the central line of the joined pieces. All the process parameters were held constant during the welding. The welding parameters in the plunge phase were as follows: The plunge speed was 12 mm/min, the plunge depth of the pin was 4.9 mm, the plunge depth of the shoulder was 0.2 mm, the rotation speed was 400 r/min, the plunge time was 24.5 s. The welding parameters in the linear welding phase were as follows: the plunge depth of the shoulder was 0.2 mm, the rotation speed was 400 r/min, and the welding speed was 24 m/min. The welded experimental panel, whose appearance after the welding is presented, was tested on a hypersonic device with a flat probe and with the beam-transmission direction going from the bottom side towards the face of the metal weld in order to find any possible occurrence of a metal discontinuity in the sample.

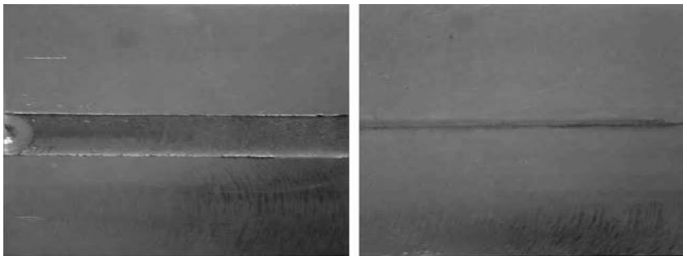

Fig 4 Photographic presentation of the face and reverse of welded joint

2.3 Base materials

In the current investigation, two aluminium alloys widely used in welding fabrication were studied, namely, the AI 5083 aluminium alloy (non-heat treatable), supplied in plates of 4 and 6 mm thickness, and the AI 7075 aluminium alloy (heat treatable, supplied in plates of 3 and 6 mm thickness. These base materials have markedly different mechanical behaviours, where their corresponding tensile stress–strain curves. From these curves it is possible to conclude that, for each base material, the mechanical properties are consistent although they were supplied in plates of different thicknesses, and so were from different batches. If the curves plotted in Fig. 5 are compared, it is possible to conclude that the AI 5083 alloy, with 148 MPa yield strength, is much softer than the AI 7075 alloy, with 290 MPa yield strength. However, despite being softer, the AA 5083 exhibits strong Portevin–Le Chaˆ telier effect and pronounced hardening with plastic deformation, attaining tensile strength values close to that of the AI 7075 alloy. This pronounced difference in plastic deformation behavior will naturally influence the FSW weldability of both types of alloys.

Table 2 Process Parameters

Alloy	Plate Type	Welding speed v, mm mm^{-1}			Rotation Speed w rev mm^{-1}			Vertical force F_z kN		
AI 5083	6-3	800	850	1100	1000	1150	1300	5	7	9
	5-4	300	400	500	400	500	600	7	11	15
	6-6	200	275	350	300	400	500	10	15	20
	5-6	200	275	350	300	400	500	10	15	20
AI 7075	6-3	800	850	1100	1000	1150	1300	7	9	11
	5-4	300	400	500	400	500	600	9	13	18
	6-6	200	275	350	300	400	500	12	17	23
	5-6	200	275	350	300	400	500	12	17	25

Table 3 Mechanical characteristics of the welded joints of AI 5083 and AI 7075

Alloys	Total number	Mechanical properties		
		$R_{0.2}$/MPa	R_m/MPa	Al %
AI 5083	1	384	522	9.5
AI 7075	1	413	548	9.8

The yield point is an apparent value measured at the elongation of 0.2 %. The tensile strength of a welded joint is about 20 % lower than that of the parent

material and the apparent yield stress is almost a third bigger in the parent material than in a welded joint. The crack location of a specimen on the tension test is situated in the transition zone going from the nugget to the remaining zone of the thermomechanically affected zone.

2.4 Microstructural evaluation

Due to the etching in the Keller's reagent, the macrostructure of the welded metal was clearly differentiated.

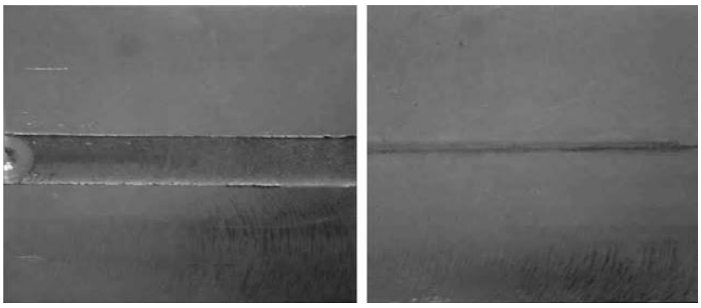

Fig 5 Photographic presentation of the face and the reverse plate alloys

The advancing and the retreating sides of the two regions, right and left from the centre of the welded joint, are also clearly visible. These are the side, where the directions of the tool-rotation vector and the welding-speed vector overlap, and the side where they have opposite directions. The macrostructure consists of the thermomechanically affected zone, the heat affected zone and the base metal zone, The thermomechanically affected zone (TMAZ) has two recognizable areas: the weld nugget and the weld root although there are authors who consider the nugget zone to be separate from the welded joint.

3. RESULTS AND DISCUSSION

3.1 Process Parameters Optimization

The variation of normal load, traverse load, and spindle torque with respect to time during the experimental trials for FSW of AI 5083- AI 7075 is studied. From the friction stir welding experiments for dissimilar combination of AI 5083 and AI 7075, it was noticed that the normal load experienced by the tool varied in the range 3.5–7 kN at rotation speed of 1120 rpm. Whereas at a higher rotation speed of 1400 rpm, the normal load was found to decrease and was in the range 3.5–6 kN. It was found that during FSW AI 5083-AI 7075 trials, the normal load was less at higher rotation speed of 1400 rpm. However no conclusive statement can be made for the normal load at rotation speed of 1120 rpm. The traverse load was in the range 0.6–1.2 kN and 0.7–1.3 kN for rotation speeds of 1120 and 1400 rpm, respectively. The spindle torque decreases with an increase in the rotation speed. Spindle torque values in the traversing phase were in the range of 33–38 Nm at 1120 rpm and 25–30 Nm at 1400 rpm. Further, it was observed that for a particular rotation speed, the spindle torque was not affected with the variation in traverse speeds (60, 80, and 100 mm/min).

3.2 Microstructural Characterization

A motif of the optical images of the cross-section of a FSW AI 5083- AI 7075 specimen. The different regions of the dissimilar friction stir weld are marked in the figure. It can be noticed that the interface between AI 5083 and AI 7075, which initially was linear prior to welding, now has a nonlinear, wavy, and distorted appearance.

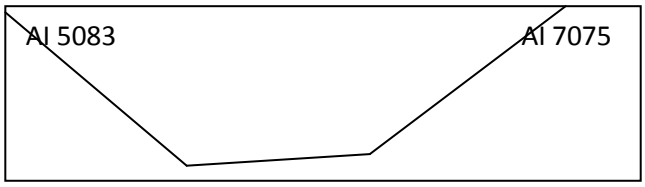

Fig 6 Motif of optical images of the transverse cross section of FSW AI 5083 and AI 707 specimen showing the various regions

The low magnification optical micrograph of the AI 5083 and AI7075 specimen. A secondary electron image of a region in the nugget denoted by the rectangle "X" .Line AB in the midthickness region shows the location of microhardness profile across the crosssection of friction stir welded AI 5083 and AI 7075 specimen. Similarly line PQ in Fig 8 shows the location of the line profile analysis for Al Kα, Mg Kα and Si Kα, across the AI 5083 and AI7075 interface. It was noticed that the width of interdiffusion was approximately 80 μm, for a relatively small duration of annealing. In this figure the occasional spikes in the Si Kα curve indicate the presence of Si-rich second-phase particles.

3.3 Mechanical Properties Evaluation

3.3.1. Microhardness.

The variation of micro hardness across the transverse cross-section of FSW AI 5083 and AI 7075

specimen in the midthickness region along line AB (shown in Figure 18 (a)). In the figure, the filled and unfilled symbols denote the micro hardness values corresponding to the regions/domains of AI 5083 and AI 7075 alloys, respectively. An abrupt transition across the AI 5083 and AI 7075 interface in the nugget was observed as one proceeds from the AI 5083 towards AI 7075. It must be noted that the micro indentation in the nugget was performed at intervals of 250 μm. From the EPMA profiles, it was observed that the width of the transition region was approximately 80 μm. Hence any possible smooth change (transition) in the micro hardness was not observed using the micro indentation technique. The micro hardness values remained nearly constant in the nugget and the adjoining HAZ for both the aluminium alloys (AI 5083 and AI 7075). Beyond the HAZ into the base material region, there was a smooth transition of the microhardness to the parent material microhardness values decreasing from the higher hardness in the nugget at the AI 7075 side and increasing from lower hardness in the nugget at the AI 5083 side.

In an earlier work reported by the authors on FSW of AI 5083, it was observed that there was a slight increase in the microhardness at the nugget-TMAZ interface on the advancing side. No such distinct rise in the microhardness was noticed at the nugget-TMAZ interface on the advancing side for the present work on FSW of AI 5083 and AI 7075.

3.3.2 Tensile Testing

The results of the tensile tests of FSW AI 5083 and AI 7075 specimens. On the abscissa, the process parameters have been arranged in the decreasing order of the weld pitch (ratio of traverse speed to rotation speed expressed in mm/rev) implying that the heat input increases as one advances from the left to right. The process parameters on the left result in lower heat input whereas the process parameters on the right have higher heat input. It was noticed that the specimen with the lowest heat input resulted in inferior tensile properties compared to the other specimen. The rest of the specimen gave good indication of strength (225MPa) where the ultimate tensile strengths were comparable and the values of the yield strengths were in the range of 135–150MPa. It was observed that the process parameters with high heat input resulted in good ductility (7%). Overall, it was observed that the use of higher rotation speeds (1400 rpm) was essential to provide good heat input and the welds thus obtained had good tensile strength. The results for the tensile testing of FSW AI 5083 and AI 7075 specimen were found to be consistent with the results obtained by Park et al. [3] for the same alloy system.

According to their results, for tool rotation and traverse speeds of 2000 rpm and 100 mm/min, respectively, the ultimate tensile strength and yield strength were 220MPa and 110MPa, respectively. However, the % elongation was found to be higher (10–17%) compared to the present study. However, the results in the present study are comparable with the work of Leitao et al. [13] on the dissimilar friction stir welding of AI 5083 and AI 7075, in which the % elongation was obtained as 8%, and the UTS and YS were 200–220MPa and 115–150MPa, respectively.

3.3.3 Mechanical testing of a welded joint

The tensile test is conducted in accordance with the standard MEST EN 10002-1:2008 on the machine INSTRON 105. The test results obtained from the specimens taken normally from the welding direction. The yield point is an apparent value measured at the elongation of 0.2 %. The tensile strength of a welded joint is about 20 % lower than that of the parent material and the apparent yield stress is almost a third bigger in the parent material than in a welded joint. The crack location of a specimen on the tension test is situated in the transition zone going from the nugget to the remaining zone of the thermomechanically affected zone.

3.3.4 Microstructural evaluation

Due to the etching in the Keller's reagent, the macrostructure of the welded metal was clearly differentiated, The advancing and the retreating sides of the two regions, right and left from the centre of the welded joint, are also clearly visible. These are the side, where the directions of the tool-rotation vector and the welding-speed vector overlap, and the side where they have opposite directions. The macrostructure consists of the thermomechanically affected zone, the heat affected zone and the base metal zone, The thermomechanically affected zone (TMAZ) has two recognizable areas: the weld nugget and the weld root although there are authors who consider the nugget zone to be separate from the welded joint, including the root as its part.

A metallographic analysis of the sample was executed with the light microscope NEOPHOT 21 having magnifications of 100-times and 1000-times. The thermomechanically affected zone in the nugget and the root region is situated at the place of the pin-tool traverse and immediately underneath its top. This is a finegrained recrystalized zone, slightly displaced toward the back side.

The remaining part of the TMAZ zone is dominantly characterized with deformed grains and its structure consists of larger grains, shown in Fig 20d. The neighbouring, heat affected zone (HAZ), is characterized with the elongated grains with little recrystallized grains and with a series of intermetallic phases, shown in Fig 20e. Its microstructure is very simillar to the microstructure of the base material.

3.4 VISUAL INSPECTION

For the plates, the energy consumed in the process was lower than that for the 5_6 welds and the results are much less dispersed, indicating weld conditions closer to equilibrium. This can be also inferred by fitting the results relative to the GOOD welds. These results show that the energy increases almost linearly with w/v, but at a much lower rate than that for the 5_6 welds.

In analyzing the results from the AI 7075 alloy, it is possible to see that with this base material the principal defect types were: flash formation, for both plate thicknesses, caused by inappropriate shoulder dimensions; internal defects, for the 6_6 plates, brought about by low tool rotation speed; and a large number of broken pin situations for the 6_3 plate, caused by excessive axial loads. Just as for the 5083 alloy, the energy values for the GOOD welds can be fitted using linear interpolation, indicating increasing values with increasing w/v ratios. For the 6_3 plates, the energy consumed is almost the same for both defective and GOOD welds, which indicates that at higher rotation speeds, which will correspond to hotter welding conditions, the process becomes very stable. On the other hand, for the 6_6 plates, energy results are more widely dispersed, especially for low w/v ratios and/or w 5300 rev min21, which correspond to colder welding conditions. As the rotation speed increases (6_3 plates), the energy consumed in the process becomes less dependent on process parameters, and is similar for both GOOD and defective welds.

3.5 DISCUSSION

The analysis of the experimental welding of the forged panels of alloys AI 5083 and AI 7075 in the state of the maximum-hardness values showed that the elongation of the welded joint is bigger than that of the parent material, which can be explained with the formation of a structure with small grains in the mixed zone.A coupled thermo-mechanical model was developed to study the temperature fields and the plunge force of alloy AI 5083 under different rotating speeds: (300, 400 and 500) r/min during the FSW process of the plunge stage. The heat transfer through the bottom surface of the welding plate is controlled with the heat transfer coefficient of 1000 W/(m2 K). A constant friction coefficient of 0.3 is assumed between the tool and the welding plate and the penalty contact method is used to model the contact interaction between the two surfaces. The heat convection coefficients on the surface of the welding of 200 °C. the temperature fields in the transverse cross-section near the tool/matrix interface after 22.8 s, when the plunge speed is 12 mm/min and the rotation speed is 400 r/min. The temperature field is symmetric.

The temperature dependence of the time for the plunge stage, when the rotation speeds are (300, 400 and 500) r/min in point T(9.5,0, 0). Numerical results indicate that the temperature in the FSW process can be increased with an increase in the rotational speed and that the maximum temperature is lower than the melting point of the welding material *T*melt = 477 °C – The maximum temperature created by the FSW ranges from 80 % to 90 % of the melting temperature of the welding material.

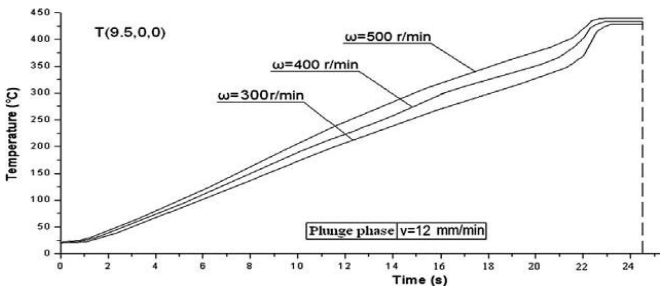

The plunge-force dependence of the time during the plunge stage of the FSW process. At the start of the FSW, during the initial plunging, due to a lack of generated heat, deformation strengthening occurs, leading to an increase of force, Pos1. After establishing the contact between the rotating pin and the welding plate, the generated heat leads to an increase in the

temperature. This temperature increase decreases the resistance to deformation, both though easier cross-slip and possible recovery and/or recrystallization. The resulting behavior is a decrease in force with a prolongation of time. This trend continues until the moment of contact between the tool shoulder and the welding plate when the force experiences a sharp increase, followed by an equally sharp decrease. The increase is related to the friction between the cold tool shoulder and the welding plate. Again cold deformation and work hardening occur prior to the heating introduced by the friction. The intense heat generation leads to a deformation under high temperatures, resulting in a decrease of the resistance to deformation, i.e. to a sharp fall of force.

4. CONCLUSION

From the results it can be concluded that high traverse speeds can be achieved in FSW of both base materials with carefully chosen process and tool parameters. In order to guarantee hot weld conditions an accurate selection of tool rotation speed is also very important. In fact, the calculation of the energy consumed in the process, as well as the analysis of the welds, shows that the process becomes relatively less dependent on process and tool parameters for high tool rotation rates. However, hot weld conditions are intimately relate AI 7075 alloy, to which higher values of plastic dissipation can be associated. The present study also shows that the establishment of accurate axial load values is also intimately related to the process parameters in use. Therefore, for cold weld conditions low axial loads led to significant internal and surface defects, whereas for hot weld conditions high axial load values led to tool destruction due to excessive plunge depth in the softened material. It was also shown that establishing suitable axial load values depends strongly on base material characteristics being advisable to perform tests in position control to determine appropriate axial load values. Finally, it was determined that the mechanical properties of the non-defective welds are relatively independent of the welding conditions. In the special case of the AI 7075 alloy, the use of very high welding speeds proved to be very effective in avoiding extra softening in the HAZ, with positive consequences in weld yield strength efficiency.

(1) Friction stir welding of dissimilar materials AA5052 and AA6061 was successfully performed. It was observed that at higher rotation speeds, the normal load and spindle torque requirement decreased.

(2) The microstructural studies suggested that there was no rigorous mixing of both materials in the nugget. There was an abrupt change in the microhardness across the interface in the nugget. However, electron probe microanalysis results stated that there was bonding at the atomic scale due to substantial interdiffusion of alloying elements at the interface of both the alloys in the nugget. Further, orientation imaging microscopy at the interfacial region suggested that despite the nonrigorous mixing and materials holding on to their domain, both the materials exhibited similar texture.

(3) Thus the interdiffusion of alloying elements and attaining of similar orientations in the nugget could have contributed to the good mechanical properties of the friction stir welded AI5083-AI 7075 specimens.

The tensile properties of the FSW AI5083-AI 7075 specimens were better than the properties of the softest of the similar friction-stir-welded systems (i.e., FSW AI 7075).The observations of the macrostructure and the microstructure clearly showed typical zones of a FSW joint made of the AI5083-AI 7075 alloy. The finest grains were observed within the nugget, while the coarsest grains were found to be in the HAZ. The ultimate tensile strength was at 80.3 % of the parent material. This behaviour is related to an intense plastic deformation influence of the heat generated due to the surface-friction plastic deformation. The temperature in the matrix under the tool must be lower than the melting temperature. The maximum temperature created by FSW ranges from 80 % to 90 % of the melting temperature of the welding material. When the rotational speed is increased, the region of high temperature can be increased. The temperature field is symmetric. After establishing the contact between the rotating pin and the welding plate, as well as the tool shoulder and the welding plate, the force starts to increase and reaches a peak value. The force drops because of the material plasticity and softens due to high stress and temperature increase. When the rotational speed is increased, the plunge force can be reduced.

REFERENCES

[1] R.S.Mishra et.al ,Friction stir welding and processing,2005 Materials Science and Engineering R50 pages 1–78.
[2] A.Forcellese et.al , Effect of process parameters on vertical forces and temperatures developed during friction stir welding of magnesium alloys,2015 ,International journal of Advanced Manufacturing technology, Volume 85, Issue 1, pages 595–604.
[3] Prakash kumar sahu, Sukhomay pal , Multi response optimization of process parameters in friction stir welded AM20 Mg alloy by taguchi grey relational analysis,2015, Journal of Magnesium and alloys vol 3 pages 36-46.
[4] Unnikrishnan M A ,Edwin Raja Dhas.j, Friction Stir welding of Magnesium alloys-A review,2015, Advances in Materials Science and Engineering, MSEJ vol 2 no 4.
[5] Barath Raj singh, A handbook on Friction stir welding Research Gate,2012, OI/10.13140/ RG.2.1.5088.6244.